



**HAL**  
open science

## Revealing the Band Structure of FAPI Quantum Dot Film and Its Interfaces with Electron and Hole Transport Layer Using Time Resolved Photoemission

Dylan Amelot, Prachi Rastogi, Bertille Martinez, Charlie Gréboval, Clément Livache, Francesco Andrea Bresciani, Junling Qu, Audrey Chu, Mayank Goyal, Sang-Soo Chee, et al.

### ► To cite this version:

Dylan Amelot, Prachi Rastogi, Bertille Martinez, Charlie Gréboval, Clément Livache, et al.. Revealing the Band Structure of FAPI Quantum Dot Film and Its Interfaces with Electron and Hole Transport Layer Using Time Resolved Photoemission. *Journal of Physical Chemistry C*, 2020, 124 (6), pp.3873-3880. 10.1021/acs.jpcc.9b10946 . hal-02514171

**HAL Id: hal-02514171**

**<https://hal.science/hal-02514171>**

Submitted on 10 Jul 2020

**HAL** is a multi-disciplinary open access archive for the deposit and dissemination of scientific research documents, whether they are published or not. The documents may come from teaching and research institutions in France or abroad, or from public or private research centers.

L'archive ouverte pluridisciplinaire **HAL**, est destinée au dépôt et à la diffusion de documents scientifiques de niveau recherche, publiés ou non, émanant des établissements d'enseignement et de recherche français ou étrangers, des laboratoires publics ou privés.

# Revealing the Band Structure of FAPI Quantum Dot Film and its Interfaces with Electron and Hole Transport Layer using Time Resolved Photoemission

Dylan Amelot<sup>1</sup>, Prachi Rastogi<sup>1</sup>, Bertille Martinez<sup>1,2</sup>, Charlie Greboval<sup>1</sup>, Clément Livache<sup>1,2</sup>, Francesco Andrea Bresciani<sup>1</sup>, Junling Qu<sup>1</sup>, Audrey Chu<sup>1</sup>, Mayank Goyal<sup>1,3</sup>, Sang-Soo Chee<sup>1</sup>, Nicolas Casaretto<sup>1</sup>, Xiang Zhen Xu<sup>2</sup>, Christophe Méthivier<sup>4</sup>, Hervé Cruguel<sup>1</sup>, Abdelkarim Ouerghi<sup>5</sup>, Angshuman Nag<sup>3</sup>, Mathieu G. Silly<sup>6</sup>, Nadine Witkovski<sup>1</sup>, Emmanuel Lhuillier<sup>1\*</sup>

<sup>1</sup> Sorbonne Université, CNRS, Institut des NanoSciences de Paris, INSP, F-75005 Paris, France.

<sup>2</sup> Laboratoire de Physique et d'Etude des Matériaux, ESPCI-Paris, PSL Research University, Sorbonne Université, CNRS UMR 8213, 10 rue Vauquelin 75005 Paris, France.

<sup>3</sup>Department of Chemistry, Indian Institute of Science Education and Research (IISER), Pune 411008, India.

<sup>4</sup> Sorbonne Université, Laboratoire de Réactivité de Surface, UMR CNRS 7197, 4 place Jussieu, F-75005 Paris, France

<sup>5</sup>Centre de Nanosciences et de Nanotechnologies, CNRS, University of Paris-Sud, Université Paris-Saclay, C2N, Palaiseau 91120, France.

<sup>6</sup>Synchrotron-SOLEIL, Saint-Aubin, BP48, F91192 Gif sur Yvette Cedex, France.

**Abstract** : Lead halide perovskite nanocrystals have attracted attention in the field of nanocrystal based light emitting diodes and solar cells, because their devices showed high performances in only a few years. Among them, CsPbI<sub>3</sub> is a promising candidate for solar cell design in spite of a too wide band gap and severe structural stability issue. Its hybrid organic-inorganic counterpart (NH<sub>2</sub>)<sub>2</sub>CHPbI<sub>3</sub> (FAPI), where the Cs is replaced with formamidinium (FA), presents a smaller band gap and also an improved structural stability. Here, we have investigated the energy landscape of pristine FAPI, and the interface of FAPI with electron and hole selective layers using transport, photoemission, and non-contact surface photovoltage by means of time-resolved photoemission. We have found from transport and photoemission that its Fermi level is deeply positioned in the band gap, enabling the material to be almost intrinsic. Time-resolved photoemission has revealed that the interface of pristine FAPI is bended toward downward side, which is consistent with a p-type nature for the interface (ie hole as majority carrier). Using TiO<sub>x</sub> and MoO<sub>x</sub> contacts, as a model for the electron and hole transport layer, respectively, allows the electron transfer from the TiO<sub>x</sub> to the FAPI and from the FAPI to the MoO<sub>x</sub>. The latter is revealed by time-resolved photoemission showing inverted band bending for the two interfaces. From these results, we clearly present the energy landscape of FAPI and its interfaces with TiO<sub>x</sub> and MoO<sub>x</sub> in the dark and under illumination. These insights are of utmost interest for the future design of FAPI based solar cell.

To whom correspondence should be sent: el@insp.upmc.fr

## INTRODUCTION

Lead halide perovskite has emerged as a promising candidate in the field of nanocrystals.<sup>1,2</sup> It becomes possible to grow bright nanocrystals<sup>3</sup> without using core/shell structure, making traditional II-VI heterostructures such as CdSe/ZnS almost obsolete.<sup>4</sup> While for perovskite thin film the solar cell has been the main targeted application<sup>5</sup>, under nanocrystal form, this is for lightning that the lead halide perovskite appears as the most promising<sup>6</sup> material. There, the defect tolerance<sup>7</sup> is used as a path to avoid surface induced trap states.

It is only later that perovskite nanocrystals have also been considered as a viable material for solar cell design. Since their synthesis was well developed for two years, CsPbI<sub>3</sub> nanocrystals already have shown superior performances than those of PbS quantum dot solar cell.<sup>8-10</sup> In spite of these tremendous improvements, perovskites nanocrystals still suffer from two main limitations which are (i) their stability (to air, light, moisture,...) and (ii) their unoptimized band gap energy. CsPbI<sub>3</sub> is certainly the most integrated material for the design of lead halide perovskite nanocrystal based solar cells,<sup>11</sup> however, its black phase (also called  $\alpha$  phase) has a band gap around 700 nm, which renders unabsorbed a significant part of the solar spectrum. Secondly, this phase is easily transformed to the yellow phase ( $\delta$  phase) which has an even larger band gap. This latter issue has been partly solved by the introduction of a better-suited ligand exchange procedure. However, the band gap remains still 300 meV too large compared with the optimal band gap of a single junction solar cell.

Narrower band gap materials will be of utmost interest. Currently, Cs/FASnI<sub>3</sub> is the narrowest band gap material reported ( $\approx$ 1000 nm) for halide perovskite<sup>12,13</sup>, but the stability issue of tin based material appears to be even more dramatic than for lead based perovskite. Formamidinium (CH<sub>5</sub>N<sub>2</sub><sup>+</sup>) lead iodide<sup>14</sup> (FAPbI<sub>3</sub>) is a hybrid material consisting organic and inorganic ions. It is currently one of the best trade-off to combine a reasonably small band gap (*i.e.* reasonably matching ideal gap to absorb solar light) with stability.<sup>15</sup>

The fine electronic structure of FAPbI<sub>3</sub> nanocrystals<sup>16</sup> at the few meV scale, has been controversial during the past years because the exact nature of the ground state (triplet vs singlet) is unclear.<sup>17-21</sup> On the other hand, at the eV scale, the electronic structure which really drives the solar cell performances needs to be better revealed. In particular, the nature of the majority carrier (electron vs hole) still remains an open question. This makes that the design of solar cell based on FAPbI<sub>3</sub> mostly follows empirical approaches.

In addition, the performance of devices based on lead halide perovskite is strongly driven by the design of interfaces.<sup>22-24</sup> Here we combine photoemission and (photo)transport measurement to demonstrate that the Fermi level of this material is located deeply within the band gap and that trap plays a limited role on charge recombination.

To further reveal the nature of the electronic states of FAPbI<sub>3</sub> nanocrystal thin film in interaction with the surrounding charge transport layers, we use a non-contact surface photovoltage measurement. This measurement is based on pump-probe photoemission to reveal *in situ* band alignment and charge transfer at the interface between FAPbI<sub>3</sub> layer and electron/hole transport layers. We reveal that hole is the majority carrier in FAPbI<sub>3</sub> nanocrystals and we present its band profile and interfaces under dark condition as well as under illumination.

## METHODS

**Chemicals:** PbI<sub>2</sub> (Alfa Aesar, 98.5%), formamidinium acetate (Fa(OAc)<sub>2</sub>, Alfa Aesar, 99%), oleylamine (OLA, Sigma-Aldrich, 80-90%), oleic acid (OA, Sigma-Aldrich), n-hexane (VWR, 99%), n-heptane (Merck, >99%), ethanol absolute anhydrous (EtOH, Carlo Erba, 99.5%), methanol (MeOH, Carlo Erba, 99.8%), toluene (VWR, 99.3%), chloroform (Carlo Erba), octadecene (ODE, Acros Organics, 90%) lead acetate (Pb(OAc)<sub>2</sub>·2Pb(OH)<sub>2</sub>, Alfa Aesar), ethyl acetate (Et(OAc)<sub>2</sub>, Carlo Erba), and titanium dioxide nanoparticles (TiO<sub>2</sub>, SOLARONIX Ti Nanoxide BL/SC)

**Preparation of stock solution of formamidinium oleate:** In a 50 mL three neck flask, 392 mg of formamidinium acetate with 18 mL of ODE and 12 mL of OA are mixed. The flask is degassed under vacuum at room temperature. Once vacuum below 1 mbar is reached, the flask is heated at 100 °C. After the salt is fully dissolved, the flask is cooled down and further degassed for 15 min.

**FAPi nanocrystal synthesis:** In a 100 mL three-neck flask, 240 mg of  $\text{PbI}_2$  are stirred in 18 mL of ODE. The flask is degassed at 110 °C under vacuum. After degassing for 20 min, 2 mL of OLA are added. Once vacuum has recovered, 1 mL of OA is added. At this point the lead salt is fully dissolved and the solution turns clear yellow. The atmosphere is switched to Ar and the temperature set at 80 °C, 20 mL of the formamidinium oleate are quickly injected. The solution turns dark red with a bright red luminescence. After 15 s the heating mantle is removed and a water bath is used to cool the flask. The solution is centrifuged at 6000 rpm. The supernatant is discarded and then the formed pellet is redispersed in hexane. Ethyl acetate is added to precipitate the particle a second time. After centrifugation the pellet is dispersed in fresh hexane.

**Ligand exchange on FAPi film:**  $\text{Pb}(\text{OAc})_2$  ligand exchange was performed on FAPi nanocrystals. A thin layer (around 20-30 nm) of the nanocrystal solution is deposited on a substrate by spin coating. Meanwhile a saturated solution of  $\text{Pb}(\text{OAc})_2$  in ethyl acetate is prepared. The solution is centrifuged and only the supernatant is saved. Then the film of FAPi nanocrystal is dipped in the previous solution for 30 s, and then rinsed in pure ethyl acetate for 30 s and subsequently annealed at 100 °C for 2 min. To build thicker films of nanocrystals, this operation can be repeated several times.

**$\text{MoO}_3$  deposition:**  $\text{MoO}_x$  layer was deposited by thermal evaporation from  $\text{MoO}_3$  powder. The samples were fixed on evaporation sample holder and introduced in thermal evaporator. Once a vacuum level of  $5 \cdot 10^{-6}$  mbar is reached,  $\text{MoO}_x$  is evaporated on the samples at a rate of  $2\text{-}3 \text{ \AA} \cdot \text{s}^{-1}$  monitored with in situ quartz crystal microbalances.

**$\text{TiO}_x$  deposition:** we use a commercial  $\text{TiO}_2$  nanocrystal solution. First, this solution was diluted by a factor of 30 with absolute ethanol. Then, the diluted solution was deposited on samples by spin coating, using the following parameters: 5000 rpm (speed)/1000 rpm  $\text{s}^{-1}$  (acceleration)/30 s (duration). The thickness of such a layer is determined to be less than 15 nm with profilometry.

**Infrared absorption:** for infrared spectroscopy, we use a Fischer Nicolet iS50 FTIR in either Attenuated Total Reflection (ATR) or in transmission configuration. The spectra are averaged over 32 acquisitions and have a  $4 \text{ cm}^{-1}$  resolution.

**UV-visible absorption:** for UV-visible spectroscopy, we use a JASCO V-730 spectrometer.

**X-ray photoemission measurements (XPS):** For photoemission spectroscopy, we use the Tempo beamline of synchrotron Soleil. Some additional core level analysis made on laboratory photoemission instrument are also provided in the supporting information. In this case an Al source is used. Films of nanocrystals are spin-casted on a gold coated Si substrate (gold layer is 80 nm thick). The ligand of the nanocrystals are exchanged using the previously described procedures.<sup>9,10</sup> Samples are introduced in the preparation chamber and degassed until vacuum below  $10^{-9}$  mbar is reached. Then samples are introduced in the analysis chamber. Photons in 60 eV to 1000 eV energy range are used. The signal is acquired onto a Scienta Ses2002 electron analyzer equipped with a delay line detector developed by Elettra<sup>25</sup>. Acquisition is done at constant pass energy within the detector. Core levels are acquired with a 100 eV pass energy, while time resolved measurements are conducted with a 200 eV pass energy. A gold substrate is used to calibrate the Fermi

energy. The absolute value of the incoming photon energy is determined by measuring the second harmonic of Pb core level peaks. Low binding energy part of the photoemission spectrum is used to determine the value of the valence band maximum with respect to the Fermi level,  $V_B - E_F$ . Then the energy of the conduction band is determined from the valence band offset of the absorption gap. Finally, the work function is determined by measuring the cut-off of secondary electrons.

## DISCUSSION

We start by synthesizing FAPI nanocrystals (NCs) with previously reported method.<sup>26</sup> The obtained NCs have a cubic shape (see transmission electron microscopy image in Figure 1b) and cubic lattice according to X-ray diffraction (Figure S1).<sup>27</sup> The band edge energy, determined from the photoluminescence spectrum is found to be 1.65 eV, see Figure 1a. The absorption spectrum is barely structured, which suggests a lack of quantum confinement in this material. The latter observation is consistent with the size of the FAPI nanoparticle (>10 nm) which is larger than the material Bohr radius (5.5 nm).<sup>28</sup>

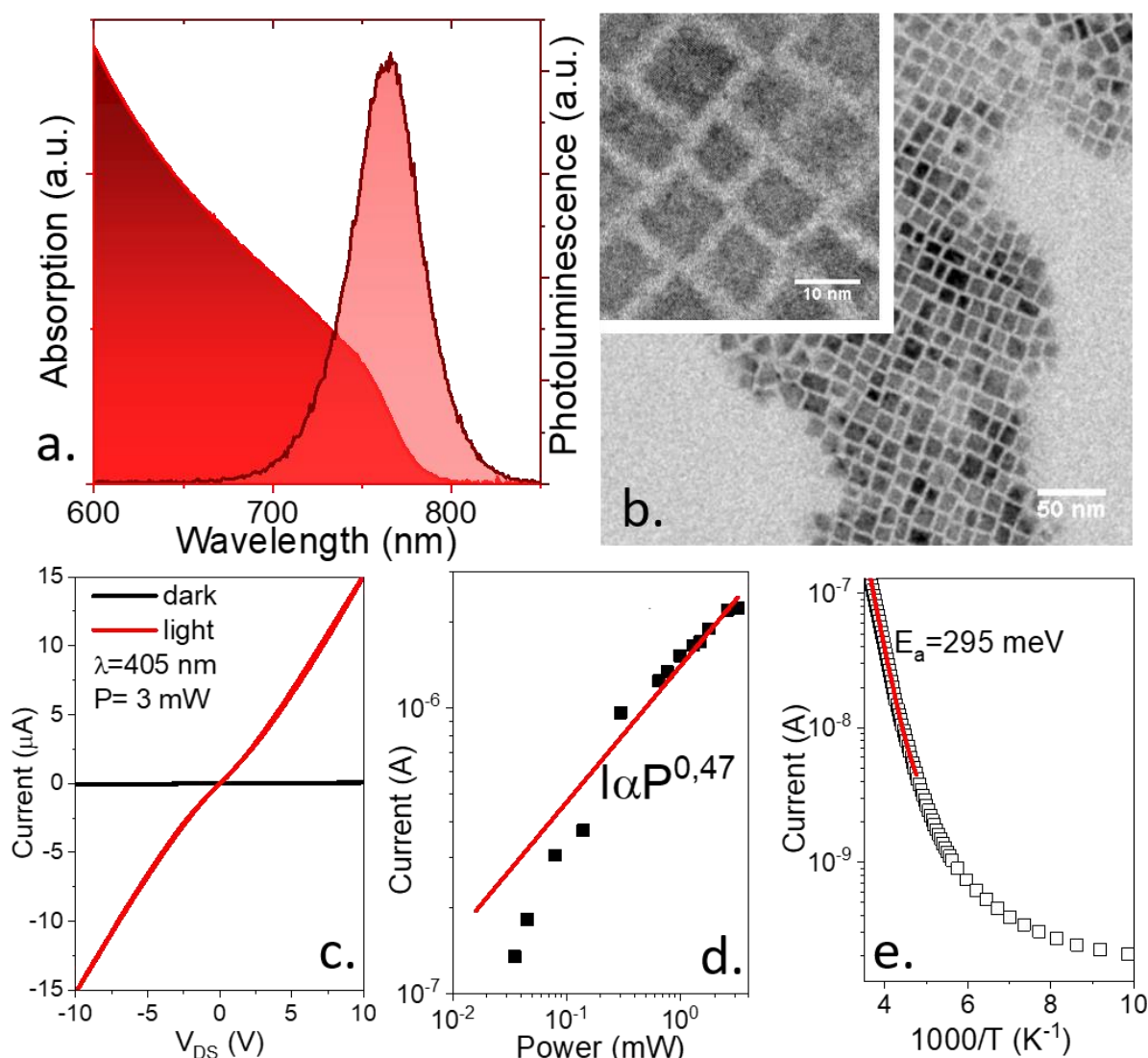


Figure 1 a. Absorption and photoluminescence spectra of a FAPI nanocrystals film. b. Transmission electron microscopy image of FAPI nanocrystals. The inset is a higher magnification image. c. I-V curves of a FAPI nanocrystals film under dark condition and under illumination ( $\lambda = 405 \text{ nm}$  and  $P = 3 \text{ mW}$ ), at room temperature. d. Current as a function of the incident power ( $\lambda = 405 \text{ nm}$ ) for a FAPI nanocrystals film. e. Current as a function of temperature for a FAPI nanocrystal film in the dark.

We then have investigated the transport properties of thin film of FAPI NCs. To render them conductive, we use the same procedure as the one developed for  $\text{CsPbI}_3$ ,<sup>8</sup> where the initial long capping ligands (oleylamine)

are stripped by dipping the film in ethyl acetate. Identical procedure is also used to prepare the film for photoemission to avoid film charging. Under illumination by a light source with photon energy larger than the band gap, we observe an increase of the conductance by two orders of magnitude, see Figure 1c. The power dependence of the current with the incident light can be reasonably fitted by a power law, of which exponent is close to  $\frac{1}{2}$ , see Figure 1d. Such dependence of the photocurrent on the incident photon flux suggests that photo-carrier generation is limited by bimolecular process (*i.e.* band to band recombination) rather than by trapping (monomolecular process).<sup>29</sup> This is consistent with previous results for transport in lead halide perovskite NC film.<sup>9</sup> The temperature dependence on the current is given in Figure 1e. The activation energy around room temperature can be obtained from an Arrhenius fit of the current, a value of 295 meV has been extracted from our measurements. In such array of NC, the transport is driven by hopping and the activation energy is mostly the result of the thermal activation of the carrier density. From this activation energy, we can conclude that the Fermi level is at least 300 meV away from any band which suggests that the Fermi level is deeply located within the band gap.

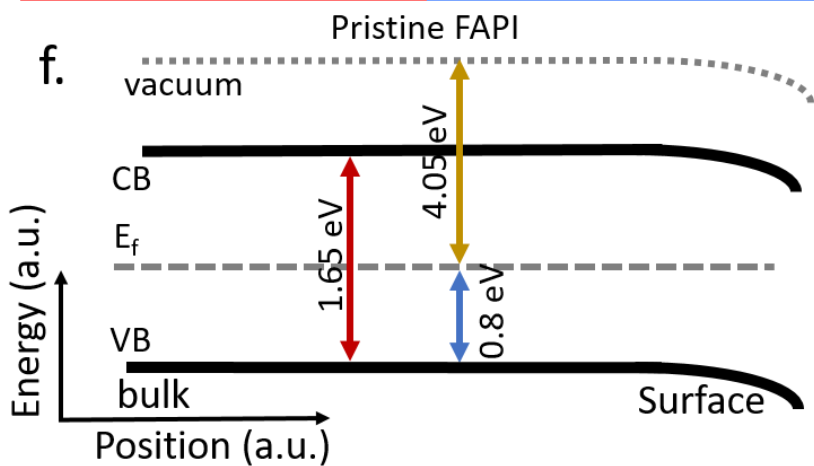
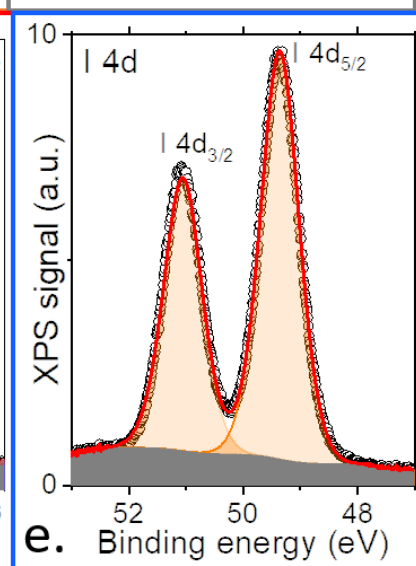
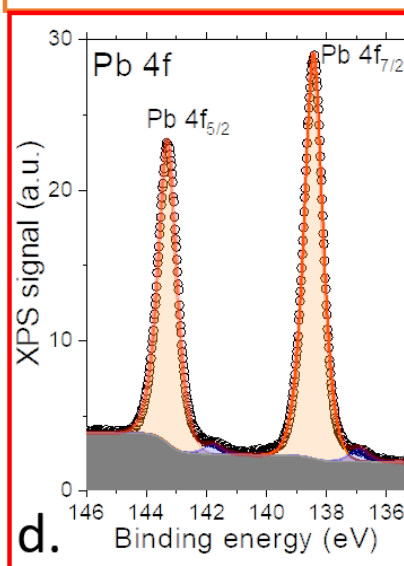
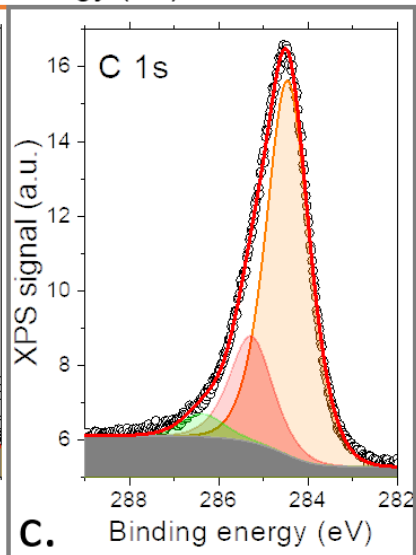
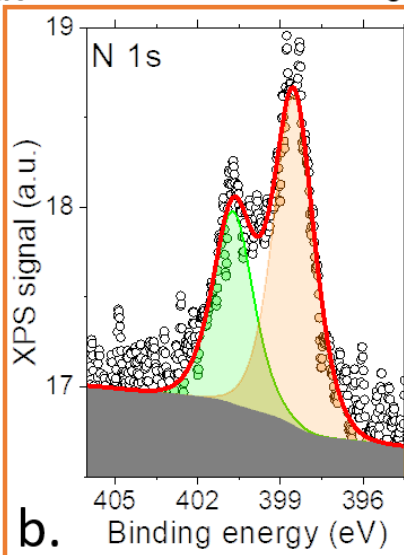
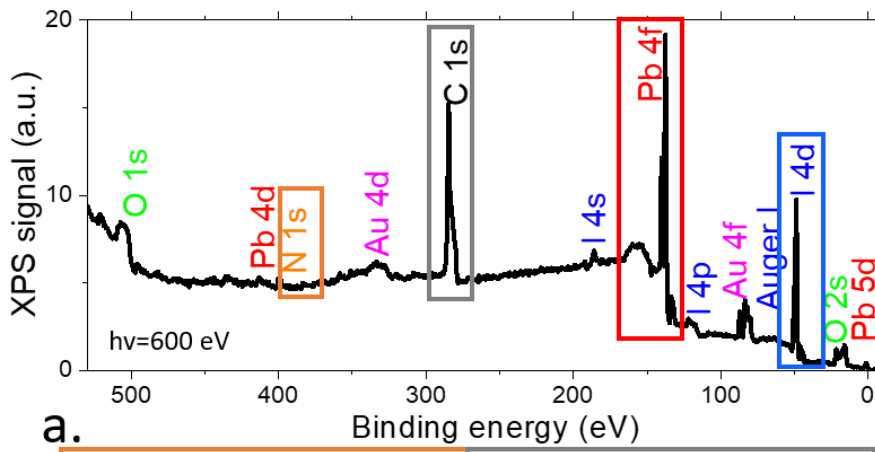


Figure 2 a. Overview of the photoemission spectrum for a FAPI nanocrystals film. The photon energy is set at 600 eV. Photoemission spectra relative to the core level of N 1s (b.), C 1s(c.), Pb 4f (d.) and I 4d (e.) states. f. Energy profile of a FAPI nanocrystals film with downward band bending at the surface as revealed by pump-probe time resolved photoemission.

The absolute energy levels of the FAPI sample are then revealed using photoemission made at Tempo beamline of Synchrotron Soleil. The sample presents contributions of C, N, Pb and I from the FAPI and a limited O contamination, see the survey spectrum in Figure 2a. The analysis of core levels is shown in Figure 2b-e. The I 4d state appears with a single contribution at a binding energy of 49.36 eV (the full width at half maximum (FWHM) is 0.79 eV, while the spin-orbit coupling (SO) is 1.7 eV). The Pb 4f state reveals two contributions appearing at 136.91 eV and 138.44 eV (FWHM = 0.73 eV, SO = 4.86 eV), which are attributed to Pb<sup>0</sup> and Pb<sup>2+</sup>, respectively. The C 1s contribution appears to have at least three contributions (BE = 284.46 eV; 285.27 eV and 286.35 eV, FWHM = 1.13 eV) which are mixtures with carbon resulting from air exposure and the one from formamidinium and ligands. The N 1s state is made of two components appearing at binding energy of 398.51 eV and 400.72 eV (FWHM = 1.74 eV). These two contributions are associated with the nitrogen from the oleylamine<sup>30</sup> used as a capping ligand and the one from the formamidinium.<sup>31</sup>

The analysis of the cut-off of the secondary electron reveals a work function of 4.05 eV, see Figure S3. Note that it is very close to the value found for CsPbI<sub>3</sub> which is  $4.1 \pm 0.05$  eV.<sup>9,32</sup> The vicinity of these two values relates to the fact that in lead halide perovskite material, the states close to the Fermi level mostly result from lead orbitals, which give rise to similar values between these two compounds.<sup>33</sup> The analysis of the valence band is generally used to determine the exact position of the Fermi level within the band gap. The Fermi level in the lower half of the band gap is associated with a p-type nature (*i.e.* hole as majority carrier), while a Fermi level in the upper part of the band gap is associated with a n-type semiconductor with electron as majority carrier. As expected, from the transport measurement, the photoemission signal reveals a Fermi level very close to the middle of the gap, see Figure 2f and S4. However, depending on the photon energy used to probe the valence band, the Fermi level can be determined just below or above the middle of the gap. In other words, the limited accuracy of the measurement and method to extract valence band maximum ( $\approx 50$  to 100 meV), prevents a clear determination of the majority carrier. In addition, the exact determination of the valence energy level becomes even more difficult once the FAPI material is coupled to metal oxide charge transport layers. Indeed, the metal oxide being defective, oxygen vacancies leads to low binding energy states (see Figure S5) which hide the semiconductor valence level.<sup>34,35</sup> Thus, alternative methods to standard photoemission are required to obtain a clear determination of the energy level profile.

To extract the clear band profile of the FAPI nanocrystals film, we conducted pump-probe photoemission measurement, of which working principle is explained in Figure 3a. A pulsed laser (640 nm) is used to generate an exciton in the semiconductor because of the photon energy being larger than the band gap of FAPI. Then, the signal from a core level (Pb 4f) using photon at 600 eV are probed. The photoemission spectrum is then collected every 10 ns. Each spectrum is fitted with two gaussians and we then follow the shift of the maximum of each gaussian as a function of time. This approach leads to higher resolution compared with static photoemission.

The signal obtained from pristine FAPI nanocrystals film is given in Figure 3b. Under illumination, we observe a decrease of 25 meV in the binding energy of the Pb 4f state. Such a decrease of the binding energy is the signature of a downward band bending as expected for a p-type semiconductor<sup>36-39</sup>. The turn-on time, see Figure 3c, is associated with the displacement of the minority carrier toward the surface, which tends to reduce the surface band bending. The duration of the electron displacement to reach a new equilibrium condition of the interface band alignment lasts for 150  $\mu$ s. Once the light is turned off, the hole then moves from the bulk and recombines with the electron accumulated at the surface under illumination. As the number of electrons at the interface will be reduced, the quasi-flat band will bend downward and finally restore the p-type interface, see Figure 3d. The decay time of the binding energy is found to be 1.4 ms and relates to the transport duration of the majority carrier to the surface. It is worth to compare the obtained majority lifetime with the one determined for PbS quantum dot which was up to recently one of the most studied material for

quantum dot-based solar cell. For PbS NCs, the turn-on and-off time have been determined to be around 63 and 210  $\mu\text{s}$ , respectively.<sup>40</sup> The longer living time obtained in FAPI suggests that there is less recombination path for carrier in FAPI than in PbS. This result is consistent with a defect tolerant character of electronic structure as expected for lead halide perovskite material.

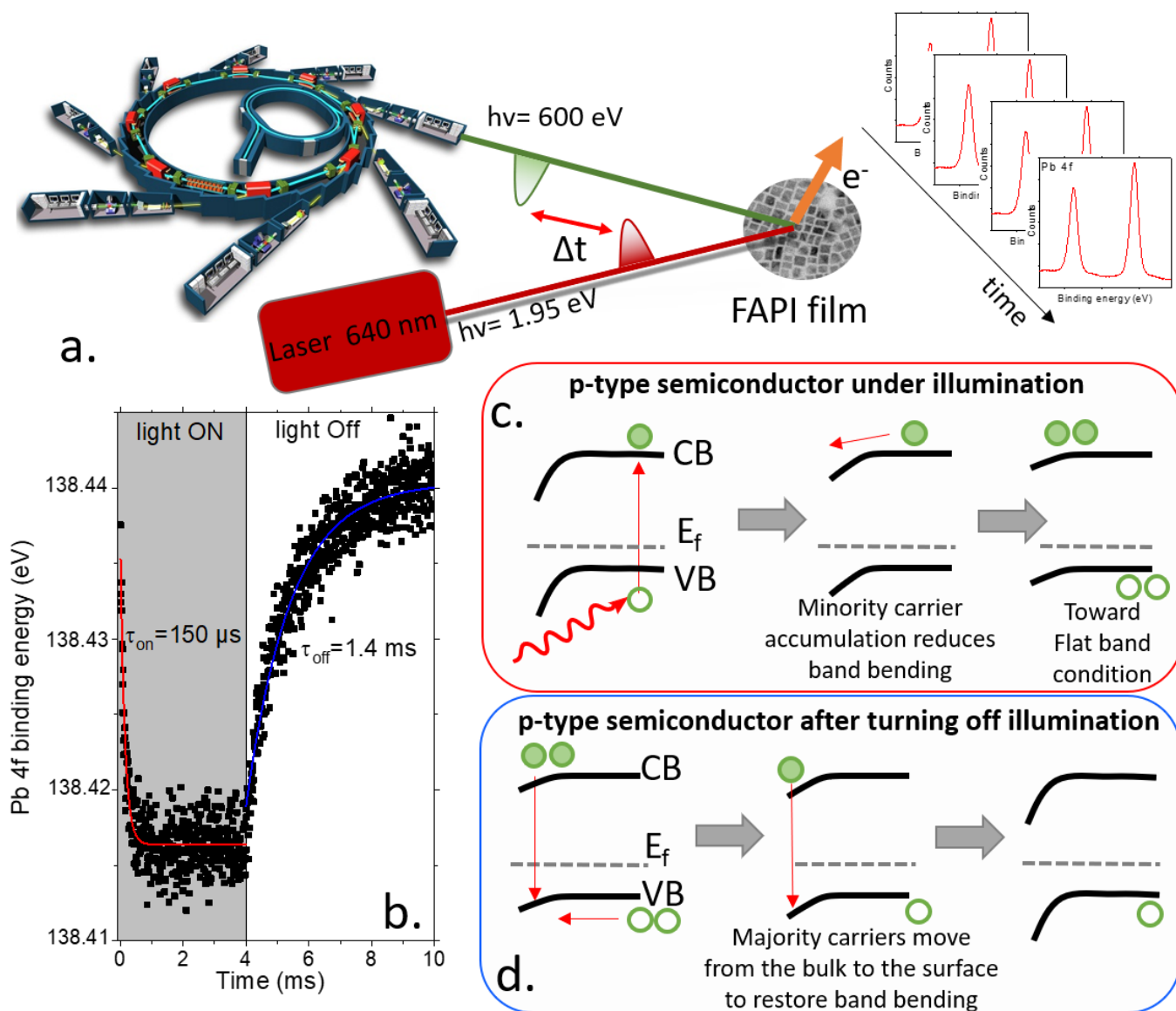


Figure 3 a. Scheme of the pump-probe photoemission experiment. A laser diode at 640 nm is used to excite the FAPI nanocrystals film, while the probe is the synchrotron beam at 600 eV. Photoemission of the Pb 4f state is then followed as a function of time. b. Energy of the Pb 4f state of FAPI nanocrystals film as a function of time, as the laser light at 640 nm is turned on and off. c. Scheme of the band bending occurring in a p-type semiconductor film under illumination and d. after the illumination is turned-off.

We then investigate the interfaces of FAPI with electron and hole transport layers, see Figure S6 for XPS overview spectra. We have chosen  $\text{TiO}_x$  and  $\text{MoO}_x$  electron and hole transport layers, respectively. A conventional diode structure<sup>10,24,41</sup> for lead halide perovskite generally includes an additional layer of spiro-OMeTAD as hole transport layer in the vicinity of the perovskite. However, because of its continuous character, the presence of such layer would have prevented the extraction of the photoelectrons. We consequently remove this layer and explore the direct effect of hole extraction layer on  $\text{MoO}_x$ . The thin layer of  $\text{TiO}_x$  is obtained by spin coating, being formed by commercial  $\text{TiO}_x$  precursor for the FAPI film, while the  $\text{MoO}_x$  layer is thermally evaporated. The atomic force microscopy represents that the FAPI film remains fairly smooth, see Figure S2. The analysis of the photoemission peak for Ti 2p and Mo 3d, are shown in Figure S7 and S8. It reveals that both materials are slightly non stoichiometric. Ti shows two oxidation states +III and

+IV state, whereas Mo exhibits three contributions from three oxidation states consisting of +IV, +V and +VI. In general, perfect stoichiometry for oxides will have required a high temperature ( $T > 300\text{ }^{\circ}\text{C}$ ) annealing step under oxygen, which would damage irreversibly the FAPI nanocrystals.

Regarding the FAPI in contact with the electron transport layer (*i.e.*  $\text{TiO}_x$ ), the time-resolved photoemission reveals a slight downward band bending (Figure 4c) at the interface evidenced by the increased Pb 4f binding energy of about 50 meV, see Figure 4a, facilitating electron extraction. Standard photoemission, Figure S7, reveals that Ti get oxidized in the presence of FAPI nanocrystals as shown by the disappearance of the +III contribution in Ti 2p components. This effect can be interpreted as an electron transfer from the  $\text{TiO}_x$  to the FAPI layer.

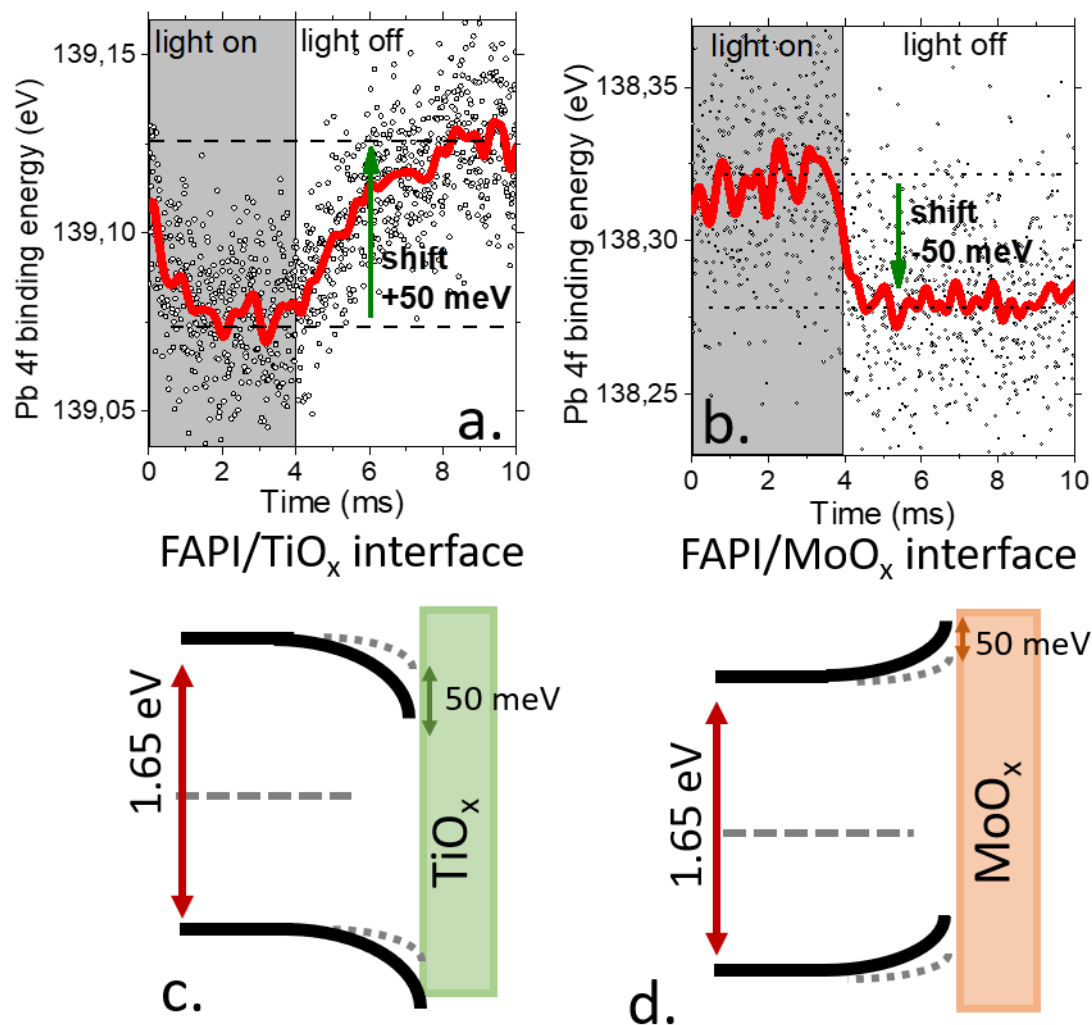


Figure 4 Binding Energy of the Pb 4f state as a function of time, during light on and off, for a FAPI nanocrystals film with a.  $\text{TiO}_2$  b.  $\text{MoO}_3$  deposited on it. In part a and b the red line is obtained by averaging the experimental points. c and d are respectively the energy profiles of a FAPI nanocrystals film and its interfaces with  $\text{TiO}_x$  and  $\text{MoO}_x$ . For interfaces, black full curves are band alignment in the dark, while dotted grey line are obtained under illumination.

Reverse effect is observed when FAPI is in contact with the hole transport layer ( $\text{MoO}_x$ ). Under illumination, time-resolved photoemission presents an inverted shift (Figure 4b), which suggests a slight upward band bending at the interface between FAPI and  $\text{MoO}_x$ , see Figure 4d. Moreover, the analysis of the Mo 3d in Figure S8, clearly shows a change in the relative weight of the different contribution of the redox state of Mo. The +V state is more favored than the +VI state, which is a signature of the  $\text{MoO}_x$  reduction suggesting an electron transfer from the FAPI to the  $\text{MoO}_x$  layer as already observed in the case of bulk methylammonium lead iodide.<sup>42</sup>

It is worth pointing that the recovery time of the dark band bending condition is typically four times longer at the MoO<sub>x</sub> interface than for the TiO<sub>x</sub> interface (380 μs for MoO<sub>x</sub> and 1.7 ms for TiO<sub>x</sub>). We can also notice that the magnitude of the light induced shift is around 50 meV for both interfaces, this is much smaller than the shift induced by the interface. From our experimental findings, we propose a full description of FAPI NCs in contact with hole and electron transport layer, in the dark and under illumination. In Figure 4c and d, FAPI NCs adopt a n-type character at the TiO<sub>x</sub> interface whereas a p-type character is given by the MoO<sub>x</sub> interface.

## CONCLUSION

To summarize, FAPI appears an interesting platform for the design of NC based solar cell because of its higher stability compared to CsPbI<sub>3</sub> and its slightly narrower band gap. Conductive film of the material can be obtained using similar method as developed for the black phase of CsPbI<sub>3</sub> (*i.e.* by stripping ligand in ethyl acetate). In addition to photoconduction, transport measurement reveals a limited role of the trap in the charge recombination and the Fermi level deep in the band gap. The latter prediction is confirmed using X-ray photoemission spectroscopy, which reveals the Fermi level is closely located to the middle of the band gap. Pump-probe time resolved photoemission reveals a p-type nature for the surface of pristine FAPI nanocrystals film. Once in presence with TiO<sub>x</sub> used as electron transport layer, the downward band bending of FAPI NCs is increased and we observe signature from an electron transfer from the TiO<sub>x</sub> to the FAPI. The reverse effect (upward band bending) is observed at the interface of FAPI NCs with MoO<sub>x</sub> used as hole transport layer. We finally propose a full description of the energy landscape of FAPI nanocrystals film and its interface with both electron and hole transport layers.

## SUPPORTING INFORMATION

Additional informations include X-ray diffraction, AFM and additional photoemission measurements.

## ACKNOWLEDGMENTS

EL thanks the support ERC starting grant blackQD (grant n° 756225). We acknowledge the use of clean-room facilities from the “Centrale de Proximité Paris-Centre”. This work has been supported by the Region Ile-de-France in the framework of DIM Nano-K (grant dopQD). This work was supported by French state funds managed by the ANR within the Investissements d'Avenir programme under reference ANR-11-IDEX-0004-02, and more specifically within the framework of the Cluster of Excellence MATISSE and also by the grant IPER-Nano, Copin, Frontal, Graskop. JQ thanks Chinese Scholar council for PhD grant while AC thanks Agence innovation defense. This work has been partially funded by the CNRS Energy unit (Cellule Energie) through the project P-NANOSOL.

## REFERENCES

- (1) Kovalenko, M. V.; Protesescu, L.; Bodnarchuk, M. I. Properties and Potential Optoelectronic Applications of Lead Halide Perovskite Nanocrystals. *Science* **2017**, *358*, 745–750.
- (2) Shamsi, J.; Urban, A. S.; Imran, M.; De Trizio, L.; Manna, L. Metal Halide Perovskite Nanocrystals: Synthesis, Post-Synthesis Modifications, and Their Optical Properties. *Chem. Rev.* **2019**, *119*, 3296–3348.
- (3) Swarnkar, A.; Chulliyil, R.; Ravi, V. K.; Irfanullah, M.; Chowdhury, A.; Nag, A. Colloidal CsPbBr<sub>3</sub> Perovskite Nanocrystals: Luminescence beyond Traditional Quantum Dots. *Angewandte Chemie International Edition* **2015**, *54*, 15424–15428.

- (4) Protesescu, L.; Yakunin, S.; Bodnarchuk, M. I.; Krieg, F.; Caputo, R.; Hendon, C. H.; Yang, R. X.; Walsh, A.; Kovalenko, M. V. Nanocrystals of Cesium Lead Halide Perovskites (CsPbX<sub>3</sub>, X = Cl, Br, and I): Novel Optoelectronic Materials Showing Bright Emission with Wide Color Gamut. *Nano Lett.* **2015**, *15*, 3692–3696.
- (5) Hodes, G. Perovskite-Based Solar Cells. *Science* **2013**, *342*, 317–318.
- (6) Yan, F.; Demir, H. V. LEDs Using Halide Perovskite Nanocrystal Emitters. *Nanoscale* **2019**, *11*, 11402–11412.
- (7) Steirer, K. X.; Schulz, P.; Teeter, G.; Stevanovic, V.; Yang, M.; Zhu, K.; Berry, J. J. Defect Tolerance in Methylammonium Lead Triiodide Perovskite. *ACS Energy Lett.* **2016**, *1*, 360–366.
- (8) Sanehira, E. M.; Marshall, A. R.; Christians, J. A.; Harvey, S. P.; Ciesielski, P. N.; Wheeler, L. M.; Schulz, P.; Lin, L. Y.; Beard, M. C.; Luther, J. M. Enhanced Mobility CsPbI<sub>3</sub> Quantum Dot Arrays for Record-Efficiency, High-Voltage Photovoltaic Cells. *Sci Adv* **2017**, *3*, eaao4204.
- (9) Mir, W. J.; Livache, C.; Goubet, N.; Martinez, B.; Jagtap, A.; Chu, A.; Coutard, N.; Cruguel, H.; Barisien, T.; Ithurria, S.; et al. Strategy to Overcome Recombination Limited Photocurrent Generation in CsPbX<sub>3</sub> Nanocrystal Arrays. *Appl. Phys. Lett.* **2018**, *112*, 113503.
- (10) Swarnkar, A.; Marshall, A. R.; Sanehira, E. M.; Chernomordik, B. D.; Moore, D. T.; Christians, J. A.; Chakrabarti, T.; Luther, J. M. Quantum Dot-Induced Phase Stabilization of  $\alpha$ -CsPbI<sub>3</sub> Perovskite for High-Efficiency Photovoltaics. *Science* **2016**, *354*, 92–95.
- (11) Ling, X.; Zhou, S.; Yuan, J.; Shi, J.; Qian, Y.; Larson, B. W.; Zhao, Q.; Qin, C.; Li, F.; Shi, G.; et al. 14.1% CsPbI<sub>3</sub> Perovskite Quantum Dot Solar Cells via Cesium Cation Passivation. *Advanced Energy Materials* **2019**, *9*, 1900721.
- (12) Jellicoe, T. C.; Richter, J. M.; Glass, H. F. J.; Tabachnyk, M.; Brady, R.; Dutton, S. E.; Rao, A.; Friend, R. H.; Credgington, D.; Greenham, N. C.; et al. Synthesis and Optical Properties of Lead-Free Cesium Tin Halide Perovskite Nanocrystals. *J. Am. Chem. Soc.* **2016**, *138*, 2941–2944.
- (13) Fang, H.-H.; Adjokatse, S.; Shao, S.; Even, J.; Loi, M. A. Long-Lived Hot-Carrier Light Emission and Large Blue Shift in Formamidinium Tin Triiodide Perovskites. *Nat Commun* **2018**, *9*, 243.
- (14) Fang, H.-H.; Protesescu, L.; Balazs, D. M.; Adjokatse, S.; Kovalenko, M. V.; Loi, M. A. Exciton Recombination in Formamidinium Lead Triiodide: Nanocrystals versus Thin Films. *Small* **2017**, *13*, 1700673.
- (15) Zhao, Q.; Hazarika, A.; Chen, X.; Harvey, S. P.; Larson, B. W.; Teeter, G. R.; Liu, J.; Song, T.; Xiao, C.; Shaw, L.; et al. High Efficiency Perovskite Quantum Dot Solar Cells with Charge Separating Heterostructure. *Nat Commun* **2019**, *10*, 2842.
- (16) Fu, M.; Tamarat, P.; Trebbia, J.-B.; Bodnarchuk, M. I.; Kovalenko, M. V.; Even, J.; Lounis, B. Unraveling Exciton-Phonon Coupling in Individual FAPbI<sub>3</sub> Nanocrystals Emitting near-Infrared Single Photons. *Nat Commun* **2018**, *9*, 3318.
- (17) Ramade, J.; Andriambariarijaona, L. M.; Steinmetz, V.; Goubet, N.; Legrand, L.; Barisien, T.; Bernardot, F.; Testelin, C.; Lhuillier, E.; Bramati, A.; et al. Fine Structure of Excitons and Electron-Hole Exchange Energy in Polymorphic CsPbBr<sub>3</sub> Single Nanocrystals. *Nanoscale* **2018**, *10*, 6393–6401.
- (18) Canneson, D.; Shornikova, E. V.; Yakovlev, D. R.; Rogge, T.; Mitioglu, A. A.; Ballottin, M. V.; Christianen, P. C. M.; Lhuillier, E.; Bayer, M.; Biadala, L. Negatively Charged and Dark Excitons in CsPbBr<sub>3</sub> Perovskite Nanocrystals Revealed by High Magnetic Fields. *Nano Lett.* **2017**, *17*, 6177–6183.
- (19) Sercel, P. C.; Lyons, J. L.; Wickramaratne, D.; Vaxenburg, R.; Bernstein, N.; Efros, A. L. Exciton Fine Structure in Perovskite Nanocrystals. *Nano Lett.* **2019**, *19*, 4068–4077.
- (20) Becker, M. A.; Vaxenburg, R.; Nedelcu, G.; Sercel, P. C.; Shabaev, A.; Mehl, M. J.; Michopoulos, J. G.; Lambrakos, S. G.; Bernstein, N.; Lyons, J. L.; et al. Bright Triplet Excitons in Caesium Lead Halide Perovskites. *Nature* **2018**, *553*, 189–193.
- (21) Tamarat, P.; Bodnarchuk, M. I.; Trebbia, J.-B.; Erni, R.; Kovalenko, M. V.; Even, J.; Lounis, B. The Ground Exciton State of Formamidinium Lead Bromide Perovskite Nanocrystals Is a Singlet Dark State. *Nat. Mater.* **2019**, *18*, 717–724.
- (22) Sanehira, E. M.; Tremolet de Villers, B. J.; Schulz, P.; Reese, M. O.; Ferrere, S.; Zhu, K.; Lin, L. Y.; Berry, J. J.; Luther, J. M. Influence of Electrode Interfaces on the Stability of Perovskite Solar Cells: Reduced Degradation Using MoO<sub>x</sub>/Al for Hole Collection. *ACS Energy Lett.* **2016**, *1*, 38–45.
- (23) Schulz, P.; Cahen, D.; Kahn, A. Halide Perovskites: Is It All about the Interfaces? *Chem. Rev.* **2019**, *119*, 3349–3417.
- (24) Hellmann, T.; Wussler, M.; Das, C.; Dachauer, R.; El-Helaly, I.; Mortan, C.; Mayer, T.; Jaegermann, W. The Difference in Electronic Structure of MAPbI<sub>3</sub> and MASnI<sub>3</sub> Perovskites and Its Effect on the Interface Alignment to the HTMs Spiro-MeOTAD and Cul. *J. Mater. Chem. C* **2019**, *7*, 5324–5332.

- (25) Bergeard, N.; Silly, M. G.; Krizmancic, D.; Chauvet, C.; Guzzo, M.; Ricaud, J. P.; Izquierdo, M.; Stebel, L.; Pittana, P.; Sergo, R.; et al. Time-Resolved Photoelectron Spectroscopy Using Synchrotron Radiation Time Structure. *J Synchrotron Rad* **2011**, *18*, 245–250.
- (26) Protesescu, L.; Yakunin, S.; Bodnarchuk, M. I.; Bertolotti, F.; Masciocchi, N.; Guagliardi, A.; Kovalenko, M. V. Monodisperse Formamidinium Lead Bromide Nanocrystals with Bright and Stable Green Photoluminescence. *J. Am. Chem. Soc.* **2016**, *138*, 14202–14205.
- (27) Protesescu, L.; Yakunin, S.; Kumar, S.; Bär, J.; Bertolotti, F.; Masciocchi, N.; Guagliardi, A.; Grotevent, M.; Shorubalko, I.; Bodnarchuk, M. I.; et al. Dismantling the “Red Wall” of Colloidal Perovskites: Highly Luminescent Formamidinium and Formamidinium–Cesium Lead Iodide Nanocrystals. *ACS Nano* **2017**, *11*, 3119–3134.
- (28) Galkowski, K.; Mitioglu, A.; Miyata, A.; Plochocka, P.; Portugall, O.; Eperon, G. E.; Wang, J. T.-W.; Stergiopoulos, T.; Stranks, S. D.; Snaith, H. J.; et al. Determination of the Exciton Binding Energy and Effective Masses for Methylammonium and Formamidinium Lead Tri-Halide Perovskite Semiconductors. *Energy Environ. Sci.* **2016**, *9*, 962–970.
- (29) Willis, L. J.; Fairfield, J. A.; Dadosh, T.; Fischbein, M. D.; Drndic, M. Controlling Nanogap Quantum Dot Photoconductivity through Optoelectronic Trap Manipulation. *Nano Lett.* **2009**, *9*, 4191–4197.
- (30) Dufour, M.; Qu, J.; Greboval, C.; Méthivier, C.; Lhuillier, E.; Ithurria, S. Halide Ligands To Release Strain in Cadmium Chalcogenide Nanoplatelets and Achieve High Brightness. *ACS Nano* **2019**, *13*, 5326–5334.
- (31) Shallcross, R. C.; Zheng, Y.; Saavedra, S. S.; Armstrong, N. R. Determining Band-Edge Energies and Morphology-Dependent Stability of Formamidinium Lead Perovskite Films Using Spectroelectrochemistry and Photoelectron Spectroscopy. *J. Am. Chem. Soc.* **2017**, *139*, 4866–4878.
- (32) Zhang, X.; Sun, C.; Zhang, Y.; Wu, H.; Ji, C.; Chuai, Y.; Wang, P.; Wen, S.; Zhang, C.; Yu, W. W. Bright Perovskite Nanocrystal Films for Efficient Light-Emitting Devices. *J. Phys. Chem. Lett.* **2016**, *7*, 4602–4610.
- (33) Lee, Y. M.; Maeng, I.; Park, J.; Song, M.; Yun, J.-H.; Jung, M.-C.; Nakamura, M. Comprehensive Understanding and Controlling the Defect Structures: An Effective Approach for Organic-Inorganic Hybrid Perovskite-Based Solar-Cell Application. *Front. Energy Res.* **2018**, *6*, 128.
- (34) Greiner, M. T.; Chai, L.; Helander, M. G.; Tang, W.-M.; Lu, Z.-H. Transition Metal Oxide Work Functions: The Influence of Cation Oxidation State and Oxygen Vacancies. *Advanced Functional Materials* **2012**, *22*, 4557–4568.
- (35) Greiner, M. T.; Lu, Z.-H. Thin-Film Metal Oxides in Organic Semiconductor Devices: Their Electronic Structures, Work Functions and Interfaces. *NPG Asia Mater* **2013**, *5*, e55.
- (36) Spencer, B. F.; Graham, D. M.; Hardman, S. J. O.; Seddon, E. A.; Cliffe, M. J.; Syres, K. L.; Thomas, A. G.; Stubbs, S. K.; Sirotti, F.; Silly, M. G.; et al. Time-Resolved Surface Photovoltage Measurements at n-Type Photovoltaic Surfaces: Si(111) and ZnO(10 $\bar{1}$ 0). *Phys. Rev. B* **2013**, *88*, 195301.
- (37) Bergeard, N.; Silly, M. G.; Krizmancic, D.; Chauvet, C.; Guzzo, M.; Ricaud, J. P.; Izquierdo, M.; Stebel, L.; Pittana, P.; Sergo, R.; et al. Time-Resolved Photoelectron Spectroscopy Using Synchrotron Radiation Time Structure. *J Synchrotron Rad* **2011**, *18*, 245–250.
- (38) Spencer, B. F.; Cliffe, M. J.; Graham, D. M.; Hardman, S. J. O.; Seddon, E. A.; Syres, K. L.; Thomas, A. G.; Sirotti, F.; Silly, M. G.; Akhtar, J.; et al. Chemically-Specific Time-Resolved Surface Photovoltage Spectroscopy: Carrier Dynamics at the Interface of Quantum Dots Attached to a Metal Oxide. *Surface Science* **2015**, *641*, 320–325.
- (39) Livache, C.; Izquierdo, E.; Martinez, B.; Dufour, M.; Pierucci, D.; Keuleyan, S.; Cruguel, H.; Becerra, L.; Fave, J. L.; Aubin, H.; et al. Charge Dynamics and Optoelectronic Properties in HgTe Colloidal Quantum Wells. *Nano Lett.* **2017**, *17*, 4067–4074.
- (40) Spencer, B. F.; Leontiadou, M. A.; Clark, P. C. J.; Williamson, A. I.; Silly, M. G.; Sirotti, F.; Fairclough, S. M.; Tsang, S. C. E.; Neo, D. C. J.; Assender, H. E.; et al. Charge Dynamics at Heterojunctions for PbS/ZnO Colloidal Quantum Dot Solar Cells Probed with Time-Resolved Surface Photovoltage Spectroscopy. *Appl. Phys. Lett.* **2016**, *108*, 091603.
- (41) Akkerman, Q. A.; Gandini, M.; Stasio, F. D.; Rastogi, P.; Palazon, F.; Bertoni, G.; Ball, J. M.; Prato, M.; Petrozza, A.; Manna, L. Strongly Emissive Perovskite Nanocrystal Inks for High-Voltage Solar Cells. *Nat Energy* **2016**, *2*, 16194.
- (42) Schulz, P.; Tjepelt, J. O.; Christians, J. A.; Levine, I.; Edri, E.; Sanehira, E. M.; Hodes, G.; Cahen, D.; Kahn, A. High-Work-Function Molybdenum Oxide Hole Extraction Contacts in Hybrid Organic–Inorganic Perovskite Solar Cells. *ACS Appl. Mater. Interfaces* **2016**, *8*, 31491–31499.

# TOC graphic

